Chapter 8
Laser Ablation Propulsion and Its Applications in Space

Claude R. Phipps

Abstract Where lasers shine is in propelling a remote object using a space-based mother ship with an onboard laser. In some cases, there is no other reasonable choice. These cases include small low Earth orbit (LEO) debris reentry, large LEO debris nudging to avoid collisions, direct launch to LEO of small payloads at low cost and raising large geosynchronous (GEO) objects to graveyard orbits. We introduce the new, exciting idea of the laser rocket, in which a "burst mode" laser accelerates a 25-kg spherical probe surrounded by a discardable ablator layer to 3.6 km/s in minutes.

8.1 What Is Laser Ablation Propulsion and What Use Is It?

People often ask me what I'm working on and their eyes glaze over when I say "laser ablation." Ablation is easy to understand. If a sufficiently intense pulsed beam hits a surface, it makes a high-temperature jet. Momentum is mass times velocity, and if the jet velocity is high, only 8 nm of material are removed each laser shot. But that small mass times the tremendous jet velocity (60 km/s) gives a lot of momentum to the surface. If a 100 ps-pulse laser beam illuminates a spot 10 cm in diameter at 1 kHz, the applied force is about 10 N on aluminum, enough to lift 1 kg.

The "Why?" for this technology is that it offers propulsion of remote objects thousands of km distant, at the speed of light. Nothing else can do that. Also, we have the option of instantly varying exhaust velocity during flight, only a matter of changing laser beam intensity. Other advantages are (a) physical separation of the energy source from the fuel, avoiding engine erosion, (b) very small minimum impulse (1nN-s), (c) instant on-off operation and (d) jet velocity which can be high compared to chemical rockets because of the higher temperatures possible in intense

C. R. Phipps (✉)
Stanford University, Stanford, CA, USA
e-mail: crphipps@aol.com

C. R. Phipps
Photonic Associates, LLC, Santa Fe, NM, USA

P. M. Ossi (ed.), *Advances in the Application of Lasers in Materials Science*,
Springer Series in Materials Science 274,
https://doi.org/10.1007/978-3-319-96845-2_8

pulsed laser absorption in surface atoms. Applications include launching small probes into Low Earth Orbit (LEO) or on interstellar journeys from LEO, and space debris re-entry or repositioning.

8.2 Photon Beam Propulsion

The laser impulse coupling coefficient C_{m} is the ratio of momentum delivered to a target to the incident beam fluence (energy per unit area) for a laser pulse, or of surface pressure to incident intensity,

$$C_{\mathrm{m}} = m_T \delta\, v_T / W = \delta \mu_E v_E / \Phi = p/I. \tag{8.1}$$

with dimensions N-s/J or N/W. C_m for pure-photon pressure is minute: the "momentum coupling coefficient" for photons reflecting off a polished surface is

$$C_{\mathrm{m}} = 2/\mathrm{c} = 6.7\ \mathrm{nN/W}. \tag{8.2}$$

A 10-kW laser reflecting perfectly would produce a thrust of only 67 μN.

The other important parameter for any type of photon propulsion is propellant exit velocity, v_{E}, simply c for light, but $\sqrt{2kT/m_i} \ll c$ for laser ablation propulsion.

Conservation of energy requires that the efficiency of the whole process is

$$\eta = \psi\, C_m v_E / 2. \tag{8.3}$$

The parameter $\psi = 1$ for photons and may be larger for ablation propulsion, as we will discuss later.

The history of photon propulsion begins 70 years ago with Tsander [1], Tsiolkovsky [2] and Oberth [3], leading to today's "solar sails." In 1953, Saenger published his concept for photon rockets [4] well before the invention of lasers.

For very long trips, where time is available, solar sails represent a practical use of pure photon propulsion. At 1 kW/m^2 at our distance from the Sun, a 10-km diameter reflective sail will generate 540 N thrust. Using this thrust, a 3 μm, 250 ton Al reflective film with this diameter could accelerate to 3 km/s in 17 days. The main problem is how to deploy such a film. Despite decades of work, the largest sail yet deployed (JAXA IKAROS [5], 2010) is 14 × 14 m.

8.3 Laser Ablation Propulsion

For usefully large forces, for example, enough to counteract gravity or accelerate a several-kg object to orbital speeds in a reasonable time, photon propulsion alone is too weak. In 1972, Kantrowitz realized [6] that the phenomenon of laser ablation could generate coupling coefficients of order 100 N/MW to 10 kN/MW, four to six

orders of magnitude larger than that for photons alone. Bunkin and Prokhorov [7] gave theory for the process in 1976.

Variable v_E is achieved by adjusting laser intensity on target—by changing focal spot area, laser pulse duration and energy—which causes exhaust velocity to vary across the range from chemical reactions (approximately 5 km/s) to much higher values easily reaching 50 km/s. This is because $v_E = (2kT_i/m_i)^{0.5}$ and 10,000 K ion temperatures T_i are readily created by a laser pulse. In short, v_E is only a matter of intensity [8]. Thrust can be varied independently of v_E by changing the laser pulse repetition rate.

After a new initiative of the Air Force Office of Scientific Research (AFOSR) and NASA, the first free flight of a 1997 laser rocket design by Myrabo [9] resulted in a flight altitude of 72 m in 2000 [10]. Delrin® (POM, a polymer) was utilized as the ablating propellant and still remains a most promising monopropellant, as we will see later. Similar investigations were reported from other countries (Russia in 1998 [11], Germany in 1999 [12], and Japan in 2001 [13].

8.4 Pulsed Laser Ablation Propulsion Details

Laser ablation propulsion operates, ideally in vacuum, by inducing a jet of vapor and plasma from a target using a high intensity laser pulse. Terminology is defined in our review of the field [14].

Ablation efficiency is defined as in (8.3), where

$$\psi = <v_x^2>/<v_x>^2 \tag{8.4}$$

It can be shown [15] that high intensity ablation plumes correspond to $\psi \leq 1.15$, so we will assume $\psi = 1$ for simplicity in discussing efficiency.

In (8.1), m_T is target mass, δv_T is the change in target velocity, W is pulse energy (J), p is surface pressure at the target, I is intensity (W/m^2), $\Phi = I\tau$ is fluence on target (J/m^2), v_E is exhaust velocity of the laser ablation jet and $\delta\mu_E$ is areal mass density (kg/m^2) in the ablation jet column created by one pulse. The change in velocity of the propelled target from a single pulse is (Fig. 8.1)

$$\delta v_T = C_m \Phi/\mu_T \tag{8.5}$$

and

$$\delta v_{T\|} = \eta_c C_m \Phi/\mu_T \tag{8.6}$$

In (8.5–8.6), μ_T is the target's areal mass density, η_c is an average geometrical efficiency factor taking account of the shape of the target and the fact that the ablation jet will be normal to each facet of its surface, not necessarily antiparallel to the laser beam. The quantity $\delta v_{T\|}$ is the change in target velocity in the beam direction.

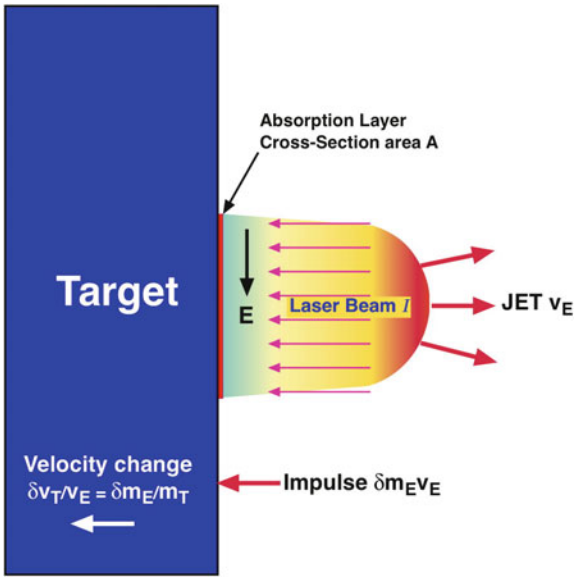

Fig. 8.1 Laser ablation impulse generation

Equation (8.6) is a numerically convenient formulation for space applications because we can deliver a fluence Φ to a region with diameter d_s and be sure that any object within that circle having mass density μ_T and the same η_c will gain the same velocity increment from that pulse. This is valid because space debris tend to exist in families with similar μ_T. For direct comparison to electric propulsion engines, the thrust to electrical power ratio is

$$C_{me} = \eta_{eo} C_m \tag{8.7}$$

Laser electrical-to-optical efficiency $\eta_{\varepsilon o}$ can range from 25 to 80%, depending on the laser type. Exhaust velocity can be determined from the product of the easily measured quantities C_m and Q (J/kg ablated) as follows. Where

$$Q = W/\delta m_T = \Phi/\delta \mu_T \tag{8.8}$$

and because $\delta\mu_T = \delta\mu_E$ by mass conservation, it can be seen dimensionally that the product $C_m Q$ must be exhaust velocity:

$$v_E = C_m Q. \tag{8.9}$$

Equation (8.3) can be extended to show that *ablation* efficiency is given by

$$\eta_{AB} = C_m v_E/2 = \delta\mu_E v_E^2/(2\,\Phi) = C_m I_{sp} g_o/2, \tag{8.10}$$

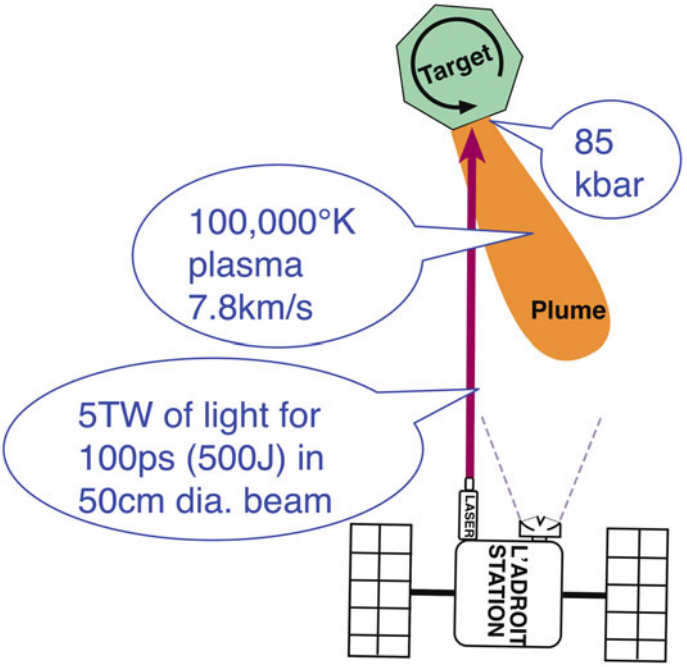

Fig. 8.2 The jet plume is always perpendicular to the surface facet. This figure gives typical parameters for the laser beam and its interaction with the target material

where g_o is the acceleration of gravity and I_{sp} is the so-called specific impulse. C_m and I_{sp} are a constant product in which I_{sp} varies inversely with C_m for engines with the same efficiency. The units of I_{sp} are seconds. The I_{sp} for light is 3.06E7 s. Another constant product is

$$C_m^2 Q/2 = \eta_{AB} \tag{8.11}$$

Because $\delta\mu_T = \rho_T \delta x$, the thickness of the target layer ablated in one pulse is (Fig. 8.2)

$$\delta x = C_m^2 \Phi/(2\rho_T \eta_{AB}) \tag{8.12}$$

For example, with an aluminum target (density $\rho_T = 2700$ kg/m^3), if $C_m = 70$ N/MW, $\Phi = 35$ kJ/m^2 and $\eta_{AB} = 1$, $\delta x = 32$ nm. At laser repetition frequency $f = 50$ Hz, even in one minute operation, total ablation depth is just 95 μm. Here we assume a perfectly uniform beam on target, such as is achievable with modern methods of apodization.

In order to determine C_m, we need laser energy W on target and impulse J (N-s) delivered to it. J can be measured using deflection of a pendulum (Fig. 8.3),

Fig. 8.3 Impulse pendulum

$$J = m_{\text{eff}}\{2g_{\text{o}}L[(1-\cos(\beta/2)]\}^{1/2} \tag{8.13}$$

In (8.13), L is the distance from the pendulum fulcrum to the point where laser impulse is generated. β is the deflection angle of a probe beam reflected from a mirror attached to the pendulum, twice the deflection angle θ. The period of a pendulum depends only on g_{o} and L, not on the mass, so that cannot be used to get impulse J.

Alternatively, one can use powerful laser interferometric techniques to get velocity directly. In either case the effective mass m_{eff} of the target-plus-pendulum must be known,

$$m_{eff} = \sum m_i L_i / L. \tag{8.14}$$

Finally, fuel usage rate is

$$\dot{m} = PC_m^2/(2\eta_{AB}). \tag{8.15}$$

The parameter Q(J/kg) is equally critical to determining the ablation efficiency η_{AB}, which governs the effectiveness of a particular laser and laser ablation fuel.

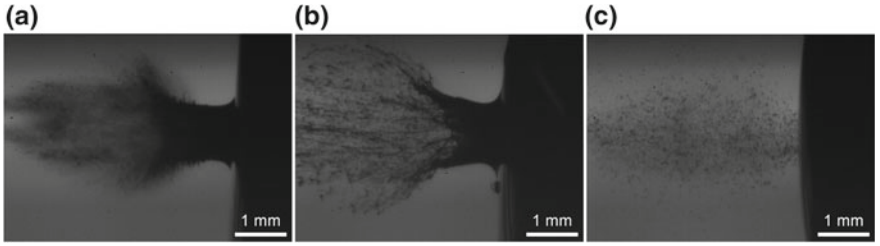

Fig. 8.4 Shadowgraph data from the Lippert group at Paul Scherer Institute shows splashing being inhibited as target viscosity increases from (**a**) to (**c**)

In principle, one may measure v_E with streak photography or Faraday probes to determine $Q = v_E/C_m$, but it is easy to miss a large mass fraction moving at very low velocity (splashing, Fig. 8.4) [16] with such techniques. Because it is difficult to measure ablated material mass with microgram accuracy from before-and-after target mass measurements, an alternative is to determine Q is from

$$Q = \Phi/(\rho_T \, \delta \, x) = 2\eta_{AB}/C_m^2 \tag{8.16}$$

by measuring the average depth δx of the ablation crater with profilometry or a similar technique. This doesn't work if the underlying material swells due to the laser pulse, a good reason to measure mass loss directly with a sensitive microbalance or by using repetitive pulses.

8.5 Optima

A first optimum is that fluence which gives maximum C_m. Figure 8.5 shows [17, 18] experimental and notional plots of C_m values versus incident fluence Φ to illustrate this optimum. In previous work, we called this maximum C_m value and the fluence at which it occurs C_{mopt} and Φ_{opt}.

For each mission, there is another kind of optimum which gives minimum energy cost to complete the mission. For example, for an Earth to LEO mission, this optimum is 100–300 N/MW [19] (Fig. 8.6). From the figure, it is clear that $C_m = 1000$ N/MW has an infinite cost for a 200 s flight (black dot at the top). In other words, the craft never reaches orbit!

In other cases, optimum performance means using an absolute minimum of ablation fuel mass, where high laser power is not a problem. This is illustrated in Fig. 8.7, from [19]. When mission duration is at a premium and laser energy is not, we have shown [20] that C_m as low as 70 N/MW is best for getting from LEO to Mars.

Our work in ablation propulsion is to find lasers and materials which achieve a desired optimum. Figure 8.6 from [19] shows how well this simple theory tracks simulations.

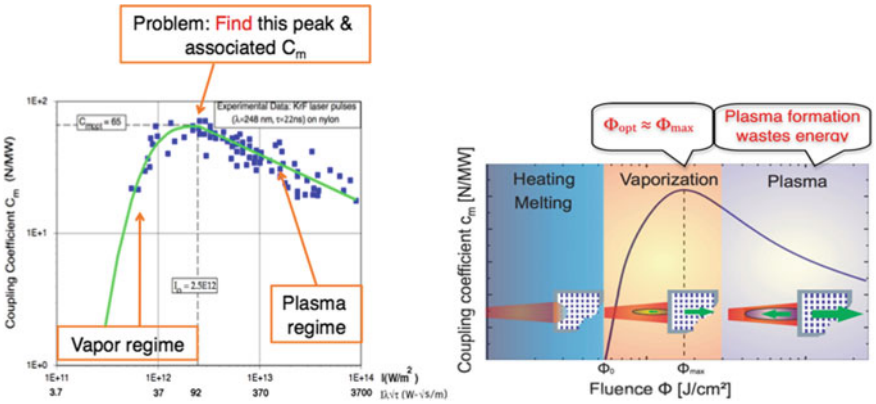

Fig. 8.5 Illustrating C_{mopt} and $\Phi_{\mathrm{opt}} = I_{\mathrm{opt}}\tau$. Clearly both vapor and plasma regime must be considered in theory to find the optimum

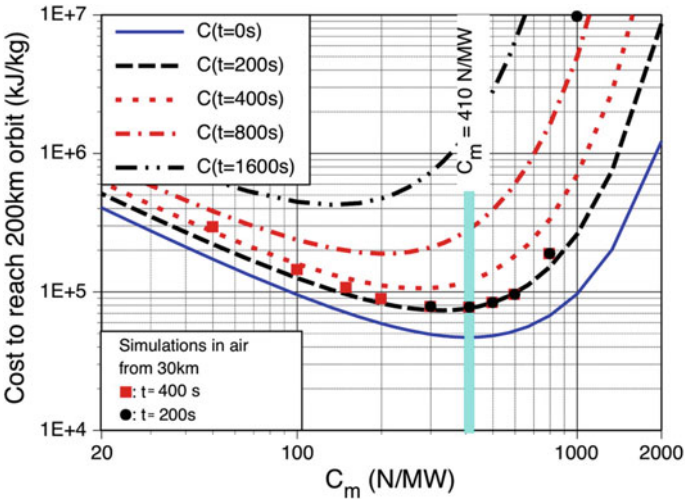

Fig. 8.6 Each mission has an optimum-cost impulse coupling coefficient. In the case studied, laser launch from 35 km to LEO, C_{mopt} is 300–500 N/MW for a 200 s flight. Lines are theory, dots are simulations for a real atmosphere. Flight time depends on laser time-average power

8.6 Why not CW?

For high efficiency in laser ablation propulsion, the laser must consist of repetitive, high intensity pulses [e.g., 20 kJ, 10 ps, 50 Hz] rather then being continuous (CW). There are several reasons for this recommendation [14]. First, high I_{sp} has not been demonstrated for CW lasers in vacuum. Second, our calculations show that intensities needed to achieve even $I_{\mathrm{sp}} = 130$ s with CW ablation (about 1 GW/m^2) require a very

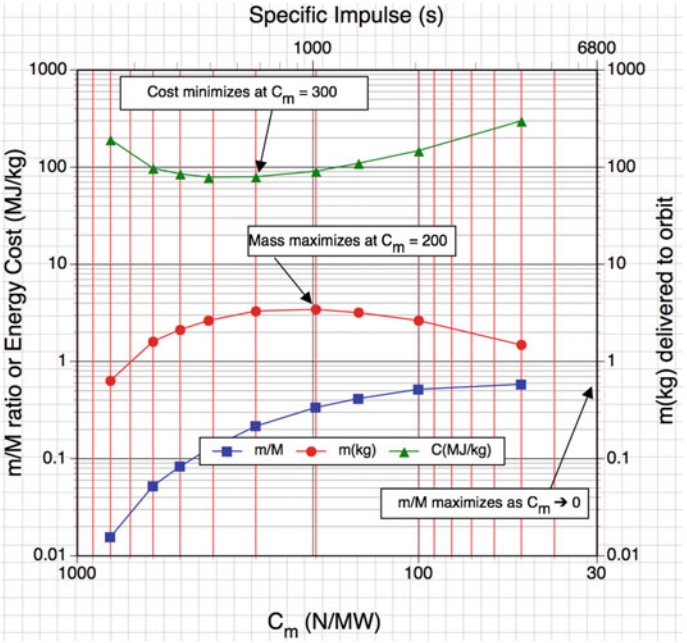

Fig. 8.7 Results of many simulations confirm the analysis, clearly showing that mass, mass ratio and cost optimize at different values of the coupling coefficient C_m. In particular, the mass ratio m/M of delivered mass m to launch mass M maximizes at $C_m = 0$ [$v_E = \infty$], mass delivered to LEO maximizes at $C_m = 200$ N/MW [$v_E = 1$ km/s] in the case studied, and cost minimizes at $C_m = 300$–400 N/MW. Here we assume $\eta_{AB} = 1$, so the exit velocity can be obtained as $v_E = 2/C_m$

small focal spot, e.g., 3.5 cm for a 1 MW laser, difficult at 200 km range or through atmospheric scintillations. In any case, CW ablation has a "welding torch" quality, generating lots of low-velocity splash [Fig. 8.5] which kills I_{sp} quickly compared to a 10 ps pulse stream, and CW laser thermal coupling will be disastrous. We will talk about this parameter later. Last, repetitive pulses give a chance for plasma clearing between shots so that refraction in the plasma jet doesn't interfere with propagation to the target. We do not emphasize CW beams for ablation propulsion in this chapter. When energy is cheap, it could play an important role.

However, nothing prevents using CW lasers to propel objects with photon pressure alone.

Because of fiber laser advances, CW lasers at 1060 nm are now readily available with 10 s of kW output power and reasonable beam quality.

Mason, et al. have proposed [21] using a 10 kW laser together with existing high-altitude telescopes (AMOS, PLATO, Mt. Stromlo) to produce displacements of a few 100 m/day for objects with $\mu \approx 10$ kg/m^2. It is worth noting, however, that the intensity delivered to the target in their proposal was only a few times the solar flux.

A higher power laser could be effective for nudging, and *laser ablation nudging* is very effective.

8.7 Breakthrough Starshot

Most recently, the "Breakthrough Starshot" concept has received venture funding. [22]. This particular proposal would require development of a 100 GW average power laser with the ability to focus dynamically on a 1 m^2 reflective sail over a distance of 4.8E6 km. This power is equivalent to that of one million 100 kW lasers. The idea would be to accelerate a 10 g nanosatellite attached to the sail to 0.27c in two minutes using photon pressure, to reach α-Centauri in 9 years. Left unanswered is how this device would communicate pictures or data back to Earth from such a distance. Assuming a 1 μm transmit wavelength, to exceed the microwave background, calculations show this would require a 1 diameter transmit antenna and a 1 km-diameter receive antenna [23] (Table 8.1).

8.8 Theory for Calculating $C_{\mathbf{mopt}}$

Because of the Fig. 8.4 behavior, in which two completely different physical regimes—vapor and plasma—meet at the optimum fluence where C_m is maximum, two distinct calculations are necessary. In the vapor regime, increasing fluence produces increasing coupling which increases without limit, while in the plasma regime, the reverse is true. Then these are combined to give the value for C_{mopt} that we want.

8.9 Plasma Regime Theory for Ablation Propulsion

Earlier work [24] resulted in a first-principle theory for C_{mp} in the plasma regime, for laser pulses longer than 100 ps and common laser wavelengths.

$$C_{mp} = p/I = 1.84E-4\left[\frac{A^{7/16}}{2^{9/16}Z^{3/8}(Z+1)^{3/16}(I\lambda\sqrt{\tau})^{1/4}}\right]N - s/J, \text{ and} \quad (8.17)$$

$$I_{spp} = 442\frac{2^{9/16}Z^{3/8}(Z+1)^{3/16}(I\lambda\sqrt{\tau})^{1/4}}{A^{7/16}}s. \quad (8.18)$$

$$T_{ep} = 2.56\frac{A^{1/8}Z^{3/4}}{(Z+1)^{5/8}}\left(I\lambda\sqrt{\tau}\right)^{1/2} \quad (8.19)$$

In the limits of this theory, $C_{mp}I_{spp} = 0.08$, and $\eta_{AB} = 0.40$. Z is the average ion charge state in the plasma plume,

Table 8.1 Breakthrough Starshot parameters

C_m (reflection)	$=2/c = 6.7E–9$
Sail area A	1 m^2
Power on sail	1E11 W
F on sail	670 N
Speed	$v = 0.27c$
Total mass	0.001 kg
Acceleration	68,000G
Accel. Interval	120 s
Distance at cutoff	4.8E6 km (0.032 AU)
Speed at cutoff	0.27c
Gamma	1.03
Laser location	On Earth
Laser wavelength	1 μm
Required aperture	5.8 km
Assumed sail mass	0.0005 kg
Thickness if Al	185 nm (650 atoms)
Al tensile strength	3E8 N/m^2
Assumed sail radius of curvature	5 m
Sail stress under pressure	9.1E9 N/m^2
Ratio of sail stress to Al tensile strength	30
Allowable heat absorption	1000 W/m^2
Needed absorptivity	1.0E-8
Goal	α Centauri
Arrival	9 years
Assumed receive aperture d_R	1.0 km
Assumed data wavelength	1 μm
Assumed data BW	0.2 μm
Assumed transmit power	1 W
Transmit dia. to match d_R	1 m
CMB noise into receiver	2.7 $\mu W/m^2/\mu m$/sterrad
Signal	9.0E-17W
S/N (signal to noise ratio)	40f

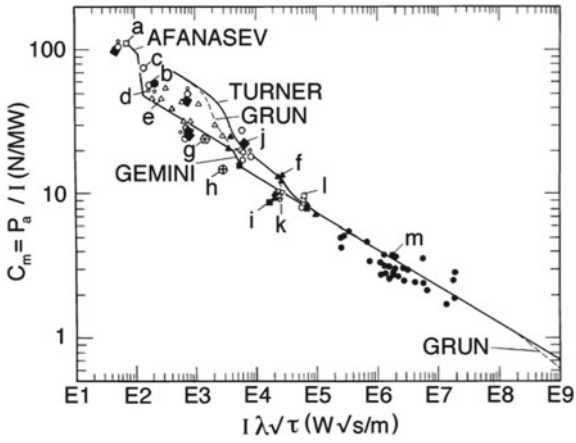

Fig. 8.8 Plasma regime data agreed with theory

$$Z = n_e / \sum_{j=1}^{j\max} (n_{ij}) \gg 1. \tag{8.20}$$

Electron density is determined by the Saha equation,

$$\frac{n_e n_j}{n_{j-1}} = \frac{2u_j}{u_{j-1}} \left(\frac{2\pi\, m_e k T_{ep}}{h^2} \right)^{3/2} \exp\left(-W_{j,j-1}/kT_{ep}\right) \tag{8.21}$$

Z is not the same as the ionization fraction $\eta_i = n_i/(n_o + n_i) \leq 1$, a function of neutral density n_o and ion density n_i.

Data from 47 datasets from the plasma regime available at that time agreed well with the plasma regime theory (Fig. 8.8).

The trick was to plot the data versus the strange parameter $I\lambda\sqrt{\tau}$, based on the functional aspects of the theory, a parameter "halfway" in its character between an intensity and a fluence. Plotting versus other variables gives a scattered result. Bumps in the figure are actually due to changing Z for simulations of each material.

8.10 Vapor Regime Theory

There are two approaches to modeling the vapor regime. The first uses tabulated pairs of pressure and temperature (p, T) from SESAME tables for some elements [25]. By equating laser intensity to energy sinks in the vapor regime, we obtain

$$I = \frac{pv}{a}\left(\frac{\gamma}{\gamma - 1}\right)\left[1 - \frac{T_o}{T} + \frac{q}{C_p T} + \frac{\gamma - 1}{2}\right] + \frac{\sigma\varepsilon}{a}T^4 + f(\tau) \tag{8.22}$$

where

$$f(\tau) = \frac{1}{a}\left[\phi(T, x_h) + \frac{x_h \rho_s C_v (T - T_o)}{\tau}\right]. \tag{8.23}$$

In (8.22) and (8.23), a is total absorption fraction of the target (not a coefficient), and ϕ is a flux limiter from inertial confinement fusion theory. We can relate the quantity p in (8.16) to T by using the Riedel equation [26] in conjunction with the SESAME equation-of-state database (e.g., for Al) maintained at Los Alamos National Laboratory for $T \leq 7890$ K, its triple point.

Equations (8.21) and (8.22) are wavelength-dependent only as λ affects the surface absorptivity a. For the infrared to ultraviolet range studied here, we have used $0.05 \leq a \leq 0.24$ for modeling aluminum [27]. Absorptivity is different from the room temperature value.

We now have a numerical solution which relates p_v and v to I over the range corresponding to our $p(T)$ data, and then compute the vapor regime coupling coefficient as $C_{mv} = p_v/I$.

Another approach is used where ablation threshold Φ_o is well-known but the (p,T) pairs are not available [28]. In this case, where $\xi = \Phi/\Phi_o$, and α [absorption coefficient (m^{-1})], is different from a in [21]. We obtained

$$C_{mv} = \sqrt{\frac{2\rho\, C^2(\xi - 1)\ln\,\xi}{\alpha\, \Phi_o \xi^2}} \text{ and} \tag{8.24}$$

$$I_{spv} = \sqrt{\frac{2\alpha \Phi_o(\xi - 1)}{\rho\, g_o^2 \ln \xi}} \tag{8.25}$$

C is a fit parameter derived by matching ablated mass density data to the expression

$$\mu = (\rho/\alpha)\ln(C\,\xi) \quad \text{kg/m}^2 \tag{8.26}$$

It is interesting to note that the $C_{mv}I_{spv}$ product from (8.19) and (8.20) give $\eta_{AB} = (g_o/2)C_{mv}I_{spv} = (2C/g_o)(1–1/\xi)$, a function which approaches $2C/g_o$ as $\xi \to \infty$. The coupling coefficient in (8.24) maximizes at $\Phi_{opt} = 4.2\ \Phi_o$, 4.2 times the threshold.

It is important to note the two quite different temperatures used in this analysis. T in, e.g., (8.22)–(8.23) is target temperature, of order 1000 K, while T_{ep}, e.g., in (8.19) and (8.21) is the plasma plume temperature and can be 100,000 K.

8.11 Combined Theory

As the caption to Fig. 8.4 points out, both vapor and plasma theory must somehow be combined to find the maximum C_{mopt} and its associated fluence. This is because

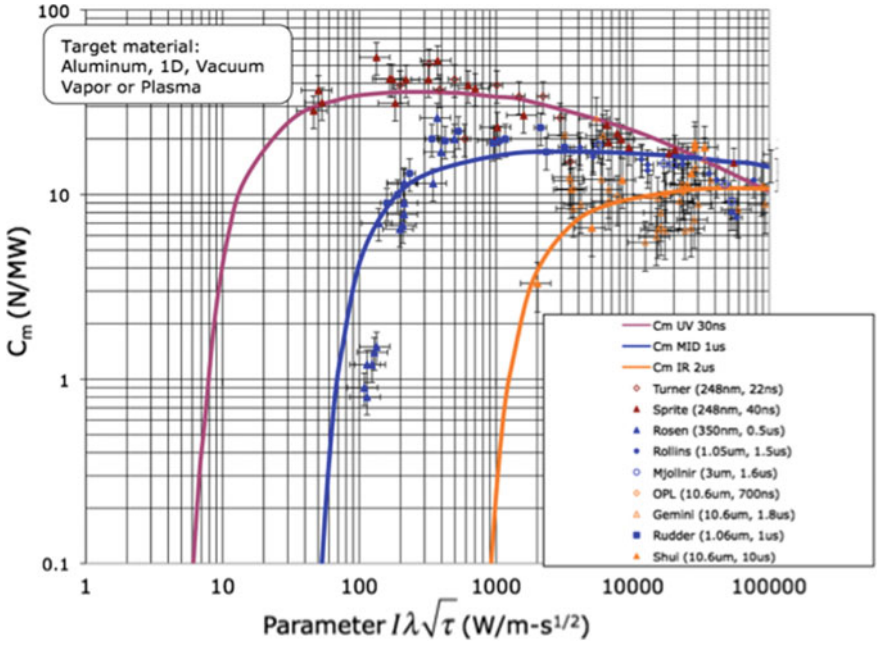

Fig. 8.9 Fitting coupling data with combined theory. Legend refers to data identified in [13]

the plasma regime C_m prediction (8.17) is infinite for zero intensity. We chose to do this with the (8.27) heuristic:

$$C_m = p/I = [(1-\eta_i)p_v + \eta_i\, p_p]/I = (1-\eta_i)\, C_{mv} + \eta_i\, C_{mp}. \tag{8.27}$$

This combination yielded a smooth transition between the two models by attenuating the vapor contribution and emphasizing the plasma contribution as ionization becomes complete using the ionization fraction η_i as a weighting function.

Combined theory specific impulse can be obtained in the same way. The combination yielded reasonable fitting of actual coupling data [29], including the C_{mopt} peak (Fig. 8.9).

It is tedious to use this method [30], because of the number of iterations required to get Z for each $I\lambda\sqrt{\tau}$. Z is a function of T through the Saha equation [31], which determines the relative population of atomic excited states. The procedure is explained in detail [25] in our 2012 paper.

An alternate approach which has less accuracy but permits rapid system design is given by Phipps and Bonnal [32]. Combining (8.17) with the trend $I\sqrt{\tau} = \mathrm{B}$ which applies for $\tau > 100$ ps gives a practical expression:

$$C_{mopt} \approx \frac{f(A,Z)}{I\lambda\sqrt{\tau}^{1/4}} = \frac{f(A,Z)}{B^{1/4}\lambda^{1/4}} = \frac{C_{exp}(A,Z)}{\lambda_{\mu m}^{1/4}} N/W. \tag{8.28}$$

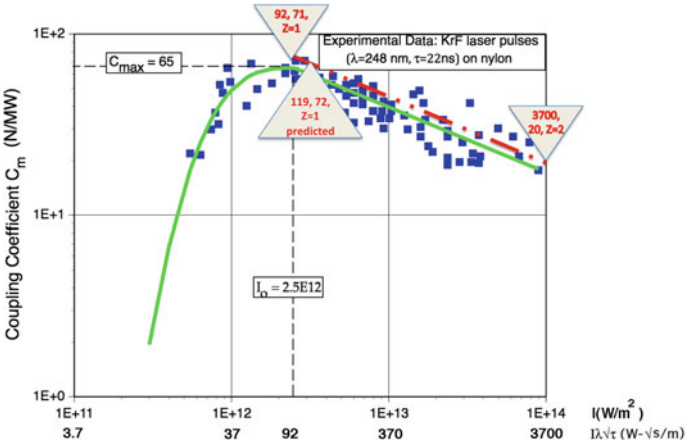

Fig. 8.10 The (8.23) approach gives the value of peak C_m *accurately*, for 22 ns pulses and its $I\lambda\sqrt{\tau}$ coordinate within a few percent

dependent only on A, Z and λ. Equation (8.28) gives a good first estimate of what C_m will be. Using B = 4.8E8 W-s$^{0.5}$/m^2 at optimum fluence,

$$\Phi_{opt} = 4.8E8\sqrt{\tau}\ \mathrm{J/m^2}. \tag{8.29}$$

and the function C_{exp} is given by

$$C_{exp}(A, Z) = 27\, A^{7/16}\, Z^{-3/8}(Z+1)^{-3/16} \quad \mathrm{N/MW}. \tag{8.30}$$

Equation (8.29) results from the fact that optimum fluence lies just above the optical breakdown threshold of the material, which varies with $\tau^{0.5}$ in 1-D thermal transfer problems [15]. Z (usually 1 or 2) can be estimated from experimental data and ionization state temperatures for a target material. This approach can give surprisingly good results (Fig. 8.10). In this case, for a 248 nm pulsed laser on nylon [33]. Because nylon has the formula $(C_{12}H_{22}N_2O_2)_n$, the correct value for the average value of A for the nylon example [in (8.30)] is 5.94.

8.12 Ultrashort Pulses

The theory on which the preceding sections are based is not valid for pulses shorter than 100 ps. To a greater and greater extent, applications we are considering use exactly that regime. Until recently, very little data existed for ultrashort pulses. For pulses in the 130–500 fs at 800 nm wavelength on Al, simulations by Fournier [34] for 530 nm and 20 ps gave $C_{mopt} = 155$ N/MW. On the other hand, other results [35,

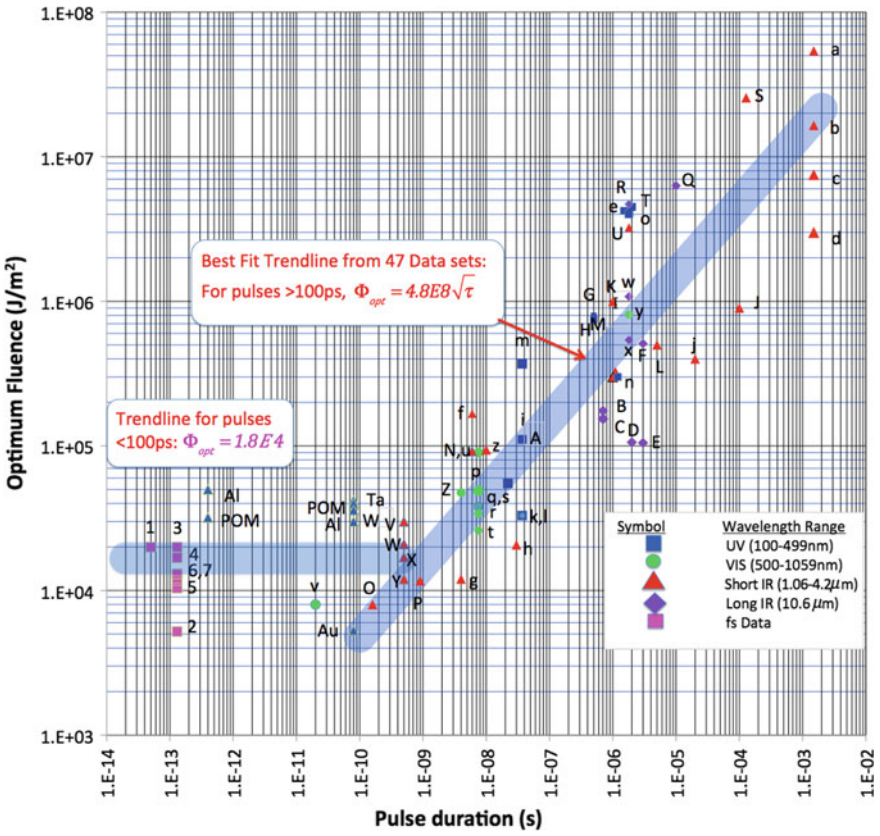

Fig. 8.11 Optimum fluence across the range 10 fs to 10 ms. New data points are blue triangles, labeled for the materials POM, Ta, W and Al. Pink squares to the left are earlier fs data. Optimum fluence for ultrashort pulses is approximately constant

36] give $C_{\mathrm{mopt}} = 35$ N/MW at 800 nm, considerably less. Scharring's simulations for circularly-polarized 1064 nm light [37] agree with this value for C_{mopt}. Figure 8.11 shows that optimum fluence for ultrashort pulses remains approximately constant below 100 ps. A complete listing of references for the data labeled with letters [14, 38, 39] would be confusing here. However, the data ranges from ms to sub-ns duration, and from 100 nm to 10.6 μm wavelength, and still follows the $\tau^{0.5}$ trend of (8.24) within a rms deviation equivalent to a factor of 1.5. This is because Φ_{opt} is usually equivalent to surface damage fluence, which is a thermal phenomenon (Table 8.2)

New data points for Al, POM, Ta, W and Au are the blue triangles [40].

In the short pulse regime, Fig. 8.12 shows the scatter in C_{m} values [17, 35, 36, 40]. The upward-slant of the trendline in the figure is due to inclusion of data at 400 fs

Table 8.2 New values for C_m and Φ_{opt} for short pulses

Pulse duration (s)	400 fs	Φ (kJ/m^2)	80 ps	Φ (kJ/m^2)
POM	125 ± 12	32 ± 6	773 ± 70	40 ± 8
Al	28 ± 3	50 ± 20	28 ± 3	30 ± 7
W	31 ± 3	260 ± 40	36 ± 7	34 ± 6
Au	–	–	37 ± 4	5.3 ± 1
Ta	–	–	29 ± 3	42 ± 8

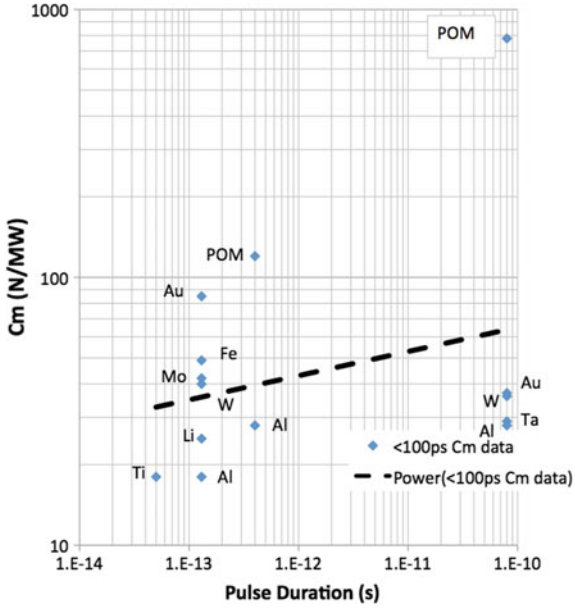

Fig. 8.12 C_m comparison. 800 nm data at 50 fs, 130 fs, 400 fs and 80 ps data. The trendline is only a guide, not based on theory

and 80 ps from the very atypical material POM, which has played a major role in 10-μm laser propulsion concepts, and is destined to do so at 1 and 0.5 μm.

The results we obtained allow making a mixture of Al powder and POM to obtain 300 N/MW, or any other value we want in the range from 30 to 770 at 80 ps. The required fluence (~30 kJ/m^2) is about the same for both materials.

8.13 Diffraction and Range as They Affect Space System Design

The goal in laser space propulsion is to get the optimum fluence—whatever it is for a particular problem—delivered to the target located at range z. The product of pulse

energy and squared effective aperture diameter WD_{eff}^2 transmitting aperture required to deliver fluence Φ at wavelength λ to a target at range z is given by

$$W D_{\text{eff}}^2 = \frac{\pi\, M^4 a_d^2 \lambda^2 z^2 \Phi}{4 T_{\text{eff}}}. \tag{8.31}$$

Diffraction causes beam spread with distance that increases linearly with wavelength and range and decreases with aperture diameter. In (8.31), a_{d} is a diffraction parameter which is 2.44 for a hard aperture and $4/\pi$ for a Gaussian radial intensity variation. M^2 is beam quality, which can be in the range 1.5–2.0 for well-designed pulsed lasers.

For example, in a case where system transmission $T_{\text{eff}} = 0.8$, in order to deliver 8 kJ/m^2 to a target at 1000 km range, the product WD_{eff}^2 must be at least 140 kJ-m^2, laser pulse energy might be 15 kJ, and the necessary effective mirror diameter D_{eff} would then be 3 m, giving a "spot size" d_{s} on target

$$d_{\text{s}} \approx a_{\text{d}} M^2 \lambda z / D_{\text{eff}}. \tag{8.32}$$

Of course we can always defocus to obtain a *larger* spot size than given by (8.32).

Equation (8.32) is an approximation because it is not accurate when $d_{\text{s}} \approx D$. In that case, it is best to compute the so-called Rayleigh range z_{R}

$$z_{\text{R}} = \pi\, w_0^2 / (M^2 \lambda) \tag{8.33}$$

and then compute beam radius away from best focus as

$$w^2(\text{z}) = w_{\text{o}}^2 \left[1 + (z/z_{\text{R}})^2\right] \tag{8.34}$$

(see Fig. 8.13). When range z is such that $2w = D_{\text{b}}$, you're done with that part of the optical system design.

8.14 Thermal Coupling with Repetitive Pulses

The *thermal* coupling coefficient $C_{\text{th}} = W_{\text{th}}/W$ is the fraction of incident laser energy that ends up as heat in the irradiated material, by whatever route. These include surface plasma reradiation and absorption, ordinary thermal conduction and mechanical stresses. It is perhaps the most important parameter that we do not know very well.

Thermal coupling data, at whatever wavelength, show a peak value of C_{th} at relatively low fluence, followed by a dramatic decrease as fluence rises toward large values, because of plasma shielding.

C_{th} is a critical parameter, because many of our applications require hundreds of thousands of pulses and even if $C_{\text{th}} = 1\%$, temperature in a 1 mm sheet of aluminum can quickly reach the melting point.

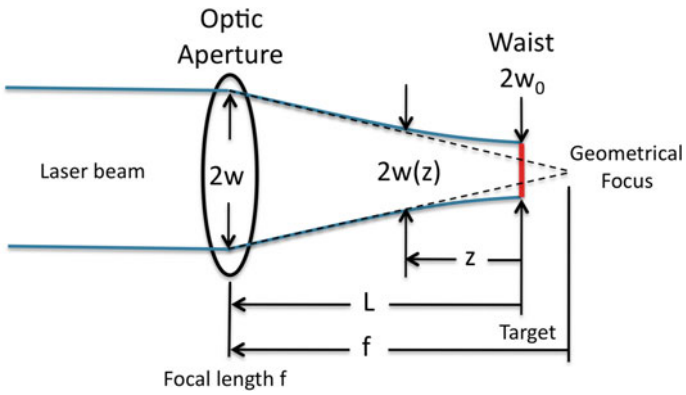

Fig. 8.13 Focusing a laser beam using an optic with aperture $D_b = 2w$

This suggests working with fs pulses, since observation of clean post-pulse features indicate low thermal coupling. Literature is full of photos of clean holes, precise ablation and no surrounding melt on targets with ultrashort pulses. However, precise C_{th} data is not available. Our instinct is to use fs pulses for minimum C_{th}, but do we really need fs pulses to be sure C_{th} is small enough?

Fortunately, Scharring has completed simulations [37] showing how C_{th} should vary with pulse duration (Fig. 8.14). The figure shows a strong advantage for ultrashort pulses as regards thermal coupling. It is clearly seen in the Figure that 10 ps single pulses at a fluence of 30 kJ/m^2 (3 J/cm^2—near optimum from our point of view) are expected to produce C_{th} of about 4% [see the "practical case" below], but longer pulses can produce C_{th} values as large as 30%.

Weber [41] shows that the maximum tolerable incident laser power P_L in an infinite string of pulses is given by

$$P_L = \frac{\Delta T_{\max} c_{\text{FOM}}}{\sqrt{f_L} a} \tag{8.35}$$

where

$$c_{\text{FOM}} = \frac{\rho c_p \sqrt{(4\pi\kappa)^3}}{5.2} \tag{8.36}$$

Taking aluminum as an example of target material and using $T_{\max} = T_{\text{melt}} = 966$ K and other parameters for aluminum, $c_{\text{FOM}} = 10.8$ and absorptivity $a = C_{\text{th}} = 1.42\%$, we find P_L=73 kW for maximum power in a continuous pulse string. Because the laser we desire for propulsion is transient rather than continuous, the laser rocket example following is still realistic, even if the average power is higher than given by (8.35).

Other materials would give different results.

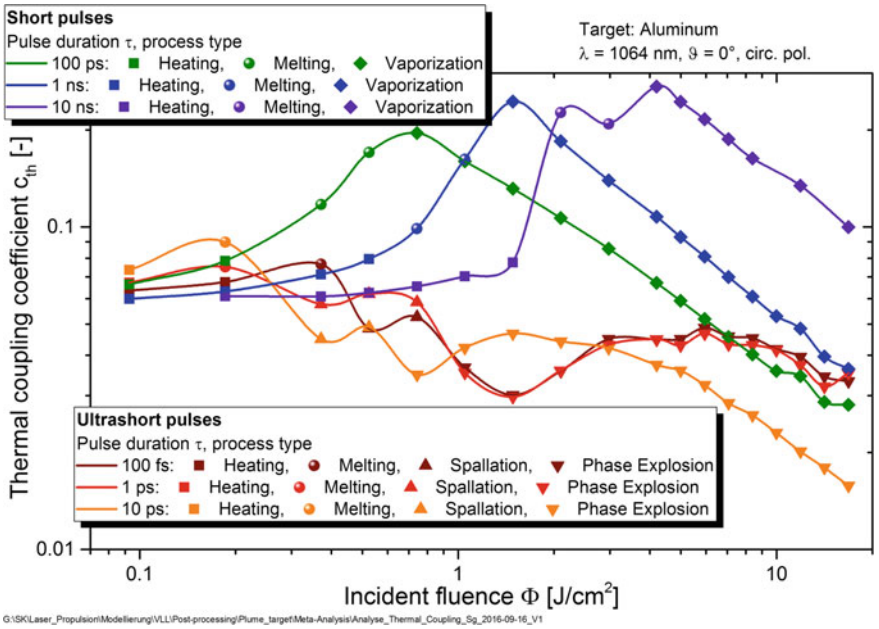

Fig. 8.14 Simulation: thermal coupling on aluminum at 1064 nm, normal incidence, circular polarization. Stefan Scharring, used by permission

8.15 Practical Case: Thermal Coupling for a Laser Rocket

In the laser rocket problem, treated in the next section, where the propelled object is a 25 kg sphere, 293 k pulses of 5 kJ are incident on the target, for a total 1.45 GJ [1.2 MW average] during an 1100 s flight. Ignoring reradiation [about 2% of incident power at T_{melt} with black body opacity], C_{th} as large as 1.4% could melt the craft. We can see that measurement of C_{th} is critical. At this time, there are no such measurements for a continuous string of ultrashort pulses.

8.16 Applications

8.16.1 Interplanetary Laser Rocket

An exciting new application is accelerating the payload in a 25 kg spherical aluminum probe from LEO to 3.6 km/s in 18 min, sufficient to achieve aphelion at Mars, with 27% mass loss (Figs. 8.15 and 8.16; Table 8.3).

Table 8.3 Parameters for Laser Rocket

Mission	Interplanetary	LEO orbit change
Parameter		
Laser wavelength	355 nm (Nd 3rd harmonic)	355 nm (Nd 3rd harmonic)
Pulse duration	100 ps	100 ps
Pulse energy	5 kJ	500 J
Probe diameter d_s	89 cm	28 cm
Probe material	Al	Al
Probe shell thickness ablated	2.7 mm	0.66 mm
Probe ablator shell mass	15 kg	15 kg
Probe mass after shell discarded	10 kg	10 kg
Pulse fluence on probe	8 kJ/m^2	8 kJ/m^2
Pulse repetition frequency	400/100 Hz	200 Hz
Pulse interval	2.5/10 ms	5 ms
Average power	2 MW/500 kW	100 kW
Optical energy in burst	1.45GJ	355 MJ
Stored in batteries	3.9GJ	1.5GJ
Battery mass	4000 kg	1520 kg
Station total mass	50,000 kg	8000 kg
Time to recharge	<1 day	<1 day
Recharge power	100 kW	17 kW
Beam quality M^2	2	2
Mirror diameter D	3 m	3 m
Rayleigh range	880 km	880 km
Used optical range	2570 km	68 km
Required aiming precision	35 nrad	4 μrad
Thickness ablated/shot	38 nm	38 nm
Assumed ablation efficiency	40%	40%
Specific impulse	816 s	816 s
Coupling coefficient C_m	70 N/MW	100 N/MW
Δv/shot	3 cm/s typ.	1.3 mm/s
Acceleration	2.6–5.3 m/s^2	0.27 m/s^2
Final probe Δv	3.6 km/s	190 m/s
Max allowable C_{th}	1.35% (incl. reradiation)	5.5% (incl. reradiation)

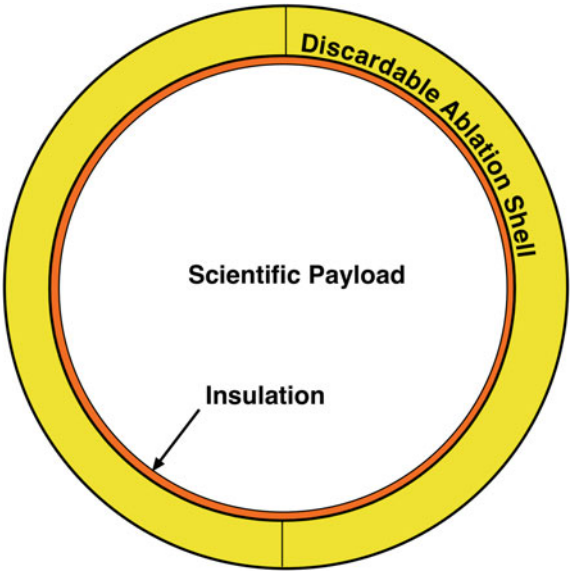

Fig. 8.15 Laser-propelled interplanetary flyer construction

In this case we create an Al/POM mixture of 5% POM and 95% Al with C_m = 70 N/MW for long propellant life. Density of the combination is 2640 kg/m^3, only slightly different from that of Al.

Maximum laser range is 1650 km. We keep the laser spot size fixed at the diffraction-limit value of 9 cm at maximum range throughout the flight, by defocusing the beam as necessary at shorter range. We use a spherical probe because Δv will always be along the laser beam axis so long as the object is centered in the beam. The probe consists of a 10 kg payload surrounded by a discardable ablator shell 2 mm thick with an internal thermal insulating layer to protect instruments during acceleration. The flyer is spinning about an axis perpendicular to the laser beam and slowly precessing so as to expose the entire surface to the laser beam. Afterward, the shell is jettisoned.

Another application is direct launch of small spacecraft from Earth to LEO using lasers. This needs MW of average power to achieve useful results. But such lasers are just around the corner.

Best efficiency is obtained from "burst mode" operation of the laser in which the laser operates at 2 MW average [5 kJ, 400 Hz] for 380 s and 500 kW for 380 s, for a total of 12.7 min. Waste heat during the burst is stored onboard the mother ship and reradiated later. We averaged σT^4 over the flight assuming a linear temperature rise to determine reradiation, which was always <2% of the total during laser illumination. Table 8.3 shows the details. The laser is more powerful than the L'ADROIT laser [42] but otherwise has similar parameters. It is powered from a battery which recharges in a day from a 100 kW array [43].

Figure 8.17 shows distance s(t), velocity v(t) and acceleration a(t) during the 18-min flight.

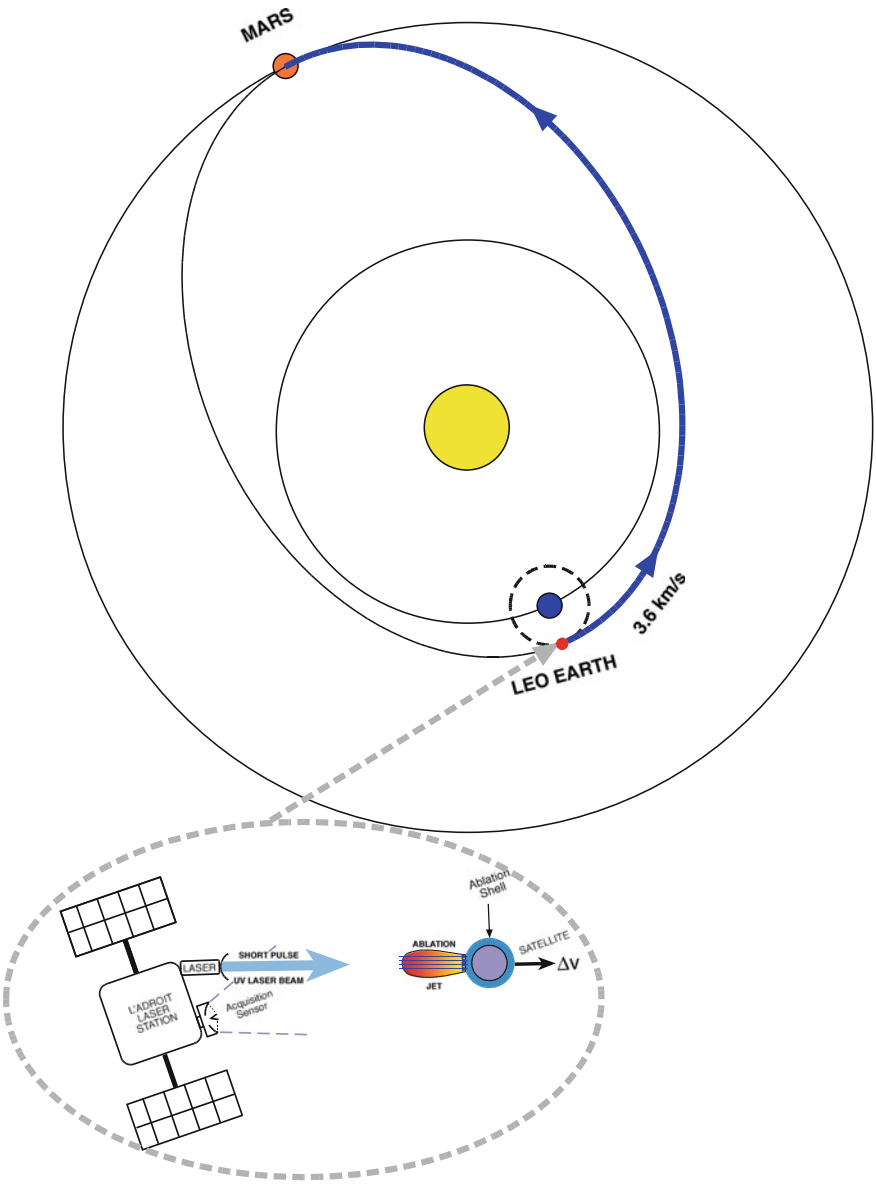

Fig. 8.16 A cis-Mars orbit starting from LEO requires $\Delta v = 3.6$ km/s

8.16.2 L'ADROIT

Remote action at the speed of light is the unique advantage of laser ablation propulsion. The L'ADROIT concept (Fig. 8.18) can generate thrust on a target 2000 km

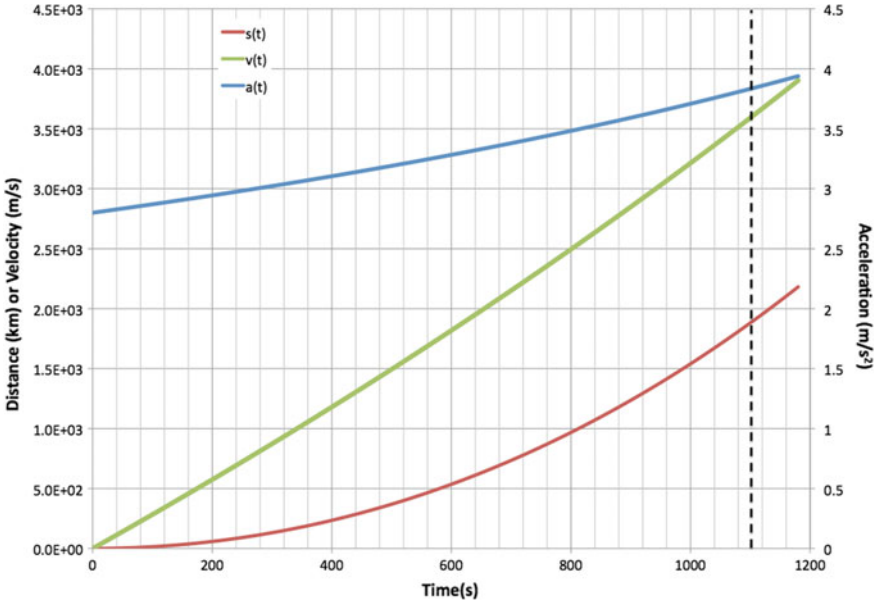

Fig. 8.17 Parameters for the cis-Mars flight from LEO. <P> = 1.25 MW [250 Hz, 5 kJ], C_m = 70 N/MW, achieving 3.6 km/s in about 18 min

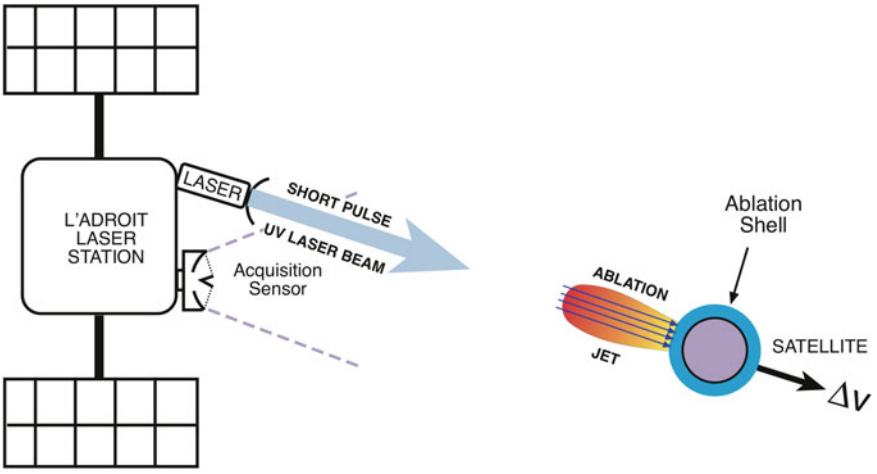

Fig. 8.18 Parameters for L'ADROIT. <P> = 21 kW [50 Hz, 400 J], causing re-entry of small LEO debris in 10 s

distant without having to be adjacent to it. This is a unique way to re-enter even tiny space debris, nudge satellites already in orbit to avoid predicted collisions, and lift derelict craft in geosynchronous orbit into higher, graveyard orbits.

L'ADROIT [42] (Laser Ablative Space Debris Removal by Orbital Impulse Transfer) was first presented at a Paris workshop in 2014 (Fig. 8.18). The laser is also operated in burst mode from batteries storing solar energy.

The version that would lift derelict geosynchronous (GEO) satellites into graveyard orbits in a day [8 kW, 3 kJ, 2.5 Hz] could raise 10 GEO satellites by 300 km in 3 months to a year, making valuable parking places in GEO available. It is a fact that 70% of objects in GEO are uncontrolled junk [32, 44].

Both laser systems operate at 355 nm wavelength (3rd Nd harmonic) with 100 ps pulses using monolithic diode-pumped Nd media. Laser electrical efficiency is about 25%.

8.16.3 Something Good for the Environment

We recently reported [45] that it is possible to directly launch small satellites to LEO from the Earth with a large ratio m/M approaching 60% of mass m delivered to orbit compared to the mass M on the ground. It requires very high time-average laser powers of 5–15 MW from kHz pulse trains of 100 ps duration at very high intensity on target (35 kJ/m^2), and a design like that in Fig. 8.15. Further, it requires a two-step launch process consisting of one power burst to get the satellite above the atmosphere, followed by a burst of 2–3 times normal power during about 60 s at the end of the flight in order to minimize excessive radial velocity, which can cause the satellite to crash at perigee (Fig. 8.19).

This technology will allow us to launch a fleet of small Earth-observing satellites in order to more carefully monitor global climate change and its consequences, in order to spot trends at the earliest possible time and to develop very highly detailed global models. Another application is to sending inspection craft to geosynchronous (GEO) orbit.

8.16.4 Fiber Laser Arrays Versus Monolithic Solid State Lasers

Giant arrays of pulsed fiber lasers are attractive alternative to monolithic laser media. The geometry of fibers makes diode pumping and heat removal more efficient. Fibers have about 100 times the energy output per kg of laser medium as monolithic solid state lasers. Figure 8.20 shows the "ICAN" [International Coherent Amplifier Network] idea [46].

However, for laser space propulsion applications, fibers have one major drawback. Progress has been slow on phasing large numbers of pulsed optical fibers (64 to date), and at least 25,000 phased fibers would be needed for ICAN to effectively deliver momentum from 100 ps pulses to objects at a distance of 100 km [47]. This is because

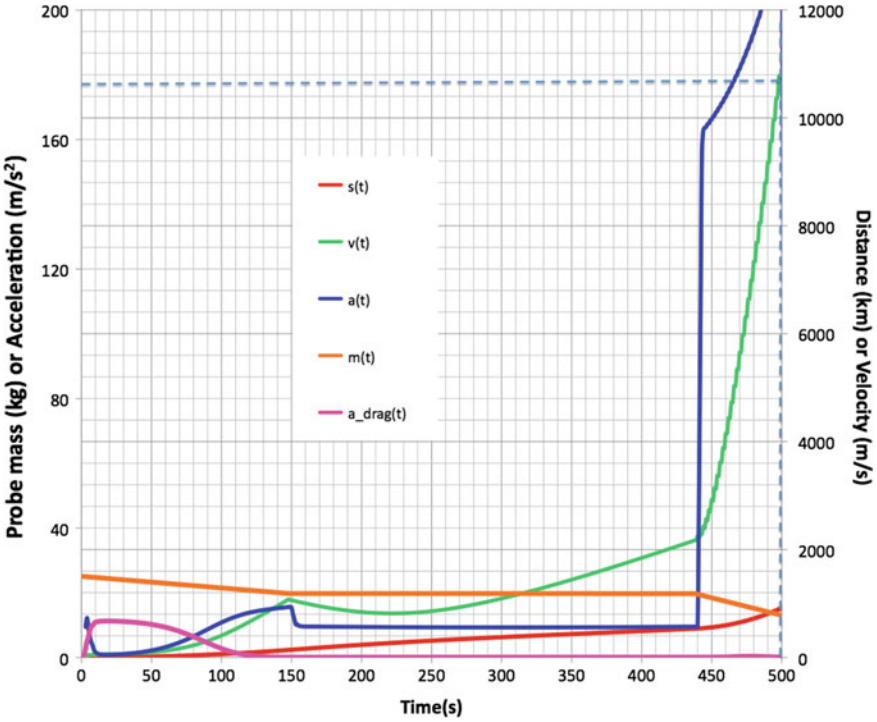

Fig. 8.19 Case 11B. Fascinating launch from ground (1 km altitude) with $C_m = 120$ N/MW. A 300 s coast followed by a 15 MW burst during 60 s at the very end gets our craft into orbit. The coast which begins at 150 s allows the craft to develop downward vertical velocity sufficient to counteract unavoidable vertical components from a groundbased laser at the end of a 1000 km flight around a curved Earth. This profile gives *m*/*M* delivered to orbit of 54% (13.5 kg). Initial zenith angle 45.5°, final zenith angle 90°. Final radial velocity is 389 m/s, final velocity 10.4 km/s. Perigee 104 km, apogee 41,700 km, 117% of geosynchronous altitude. Insertion slope is 2.12°. Minimal energy is wasted in drag, even though we are starting from the ground

we need a pulse energy of 100 J at 100 ps for this operation [to see this, apply (8.31) with $\Phi = 30$ kJ/m^2, z = 100 km, $\lambda = 355$ nm and reasonable mirror sizes]. However, a single fiber can deliver only 4 mJ without catastrophic failure due to self-focusing and other serious nonlinear optical effects under these conditions. These effects include stimulated Brillouin scattering, stimulated Raman scattering, photo-darkening and four-wave mixing.

Going from 4 phased fibers to 25,000 will be a difficult jump.

A first step to testing fibers for application to the debris problem will be forthcoming tests of debris reëntry using the EUSO telescope on board the Space Station, together with one of the ICAN fiber lasers [48].

We have learned never to say something is impossible!

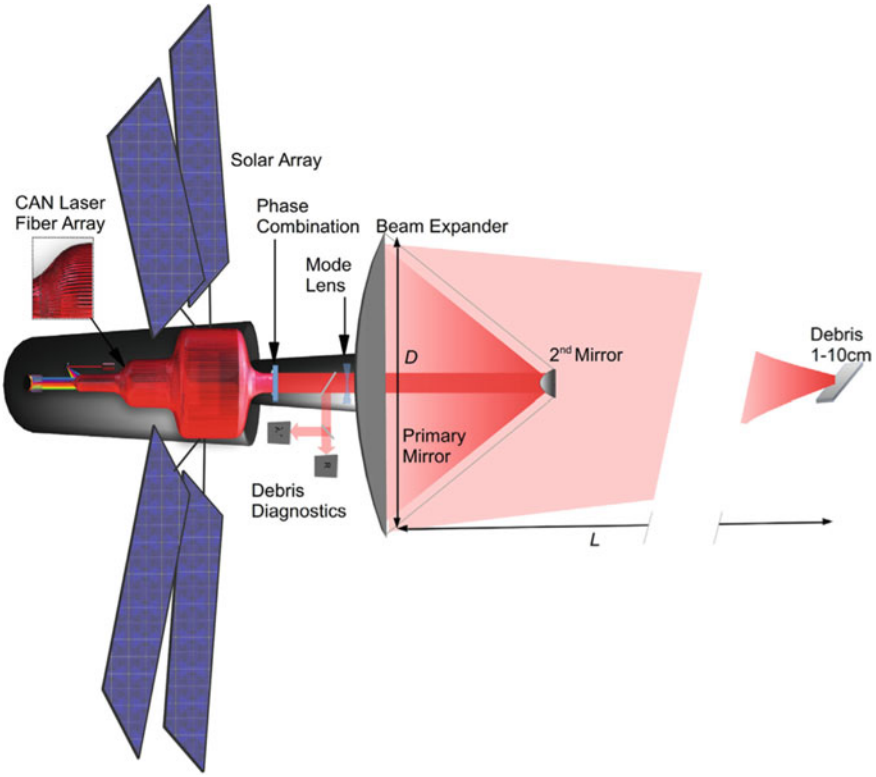

Fig. 8.20 ICAN concept

8.16.5 Repetitive Pulse Monolithic Diode Pumped Solid State Lasers

The state of the art in the lasers we currently need to achieve all of these applications is represented in the HiLASE program [49], where the Rutherford Appleton Laboratory's "DiPOLE 100" laser achieved its full design performance of 1 kW average power with 10 Hz, 100 J pulses at 10 ns pulse duration. Just a factor of 10 increase in output power will enable many of our applications in space.

8.16.6 Perspective

In this brief review, we have discussed one of the most exciting future applications of pulsed lasers. Laser ablation propulsion can re-enter space debris, nudge large satellites out of harm's way, and create a fleet of Earth-observing satellites and lift

derelict GEO stations to parking orbits. We discussed the disadvantages of CW lasers for this task. However, it is also possible that new ideas for 1 MW free-electron lasers with a format consisting of 1 MHz 1 J pulses will change this idea for refractory targets [50].

It can also get a 10 kg probe launched on its way to Mars in minutes.

We discussed the related laser-materials interaction physics in detail, and new results at 400 fs and 80 ps which will make this propulsion mode possible. Developing this capability depends on developing the associated lasers, beam directors and space stations on which they will be based. It also depends on better understanding of thermal coupling measurements under the proposed laser parameters.

References

1. F. Tsander, Flight to other planets (1924), in *Development of Russian Rocket Technology*, ed. by Y. Moshkin (Mashinostroyeniye Press, Moscow, 1973) (in Russian)
2. K. Tsiolkovsky, Plan of space exploration, 1926 (in Russian), available in English in "Exploration of the Universe with Reaction Machines: Exploring the Unknown," NASA History Series. NASA SP 4407, Washington, D.C. (1995)
3. H. Oberth, *Die Rakete zu den Planetenräumen (The Rocket to the Planet Spaces)* (Oldenbourg Verlag, München, 1923)
4. E. Sänger, Zur Theorie der Photonenraketen, in *Probleme der Weltraumforschung*, (IV. Internationaler Astronautischer Kongress, Zürich 1953; S. 32), Laubscher, Biel-Bienne (1955)
5. H. Yano, Cosmic dust detection by the IKAROS large area dust detectors ion interplanetary space from the Earth to Venus, in *42nd Lunar and Planetary Science Conference* (2011) (in Japanese)
6. A. Kantrowitz, Propulsion to orbit by ground-based lasers. Astronaut. Aeronaut. **10**(5), 74–76 (1972)
7. F.V. Bunkin, A.M. Prokhorov, Use of a laser energy source in producing a reactive thrust. Sov. Phys. Usp. **19**(7), 561–573 (1976)
8. C. Phipps, J. Luke, W. Helgeson, Laser-powered, multi-newton thrust space engine with variable specific impulse, in *High-Power Laser Ablation VII*, *Proceedings of SPIE* **7005**, 1X1–1X-8 (2008)
9. L.N. Myrabo, D.G. Messitt, F.B. Mead Jr., Ground and flight tests of a laser propelled vehicle, in paper AIAA 98-1001, *36th AIAA Aerospace Science Meeting and Exhibit*, Reno, NV 12–15 January 1998
10. L. N. Myrabo, World Record Flights of Beam-Riding Rocket Lightcraft: Demonstration of 'Disruptive' Propulsion Technology, in paper AIAA 2001-3798, *37th AIAA/ASME/ SAE/ASEE Joint Propulsion Conference*, Salt Lake City, UT, 8–11 July 2001
11. R.A. Liukonen, Laser jet propulsion, in *XII International Symposium on Gas Flow and Chemical Lasers and High-Power Laser Conference*, Proceeding of SPIE **3574**, 470–474 (1998)
12. W.L. Bohn, Laser lightcraft performance, in *High-Power Laser Ablation II*, Proceeding of SPIE **3885**, 48–53 (1999)
13. A. Sasoh, Laser-driven in-tube accelerator. Rev. Sci. Instrum. **72**(3), 1893–1898 (2001)
14. C. Phipps, M. Birkan, W. Bohn, H.-A. Eckel, H. Horisawa, T. Lippert, M. Michaelis, Y. Rezunkov, A. Sasoh, W. Schall, S. Scharring, J. Sinko, Review: laser ablation propulsion. J. Propul. Power **26**(4), 609–637 (2010)
15. C.R. Phipps, J.R. Luke, Laser Space Propulsion, in *Laser Ablation and its Applications*, Chap. 16, *Springer Series in Optical Sciences*, vol. 129, 407–434 (2007)
16. T.K.M. Lippert, Materials for laser propulsion, *SPIE* **7005** paper 7005–38 (2008)

17. C. Phipps et al., Appl. Surf. Sci. **252**, 4838–4844 (2006)
18. B. Esmiller, C. Jacquelard, H.-A. Eckel, and E. Wnuk, Space debris removal by ground-based lasers: main conclusions of the European project CLEANSPACE. Appl. Opt. **53**(31), I45–I54 (2014)
19. C. Phipps et al., Optimum parameters for laser-launching objects into low Earth orbit. Laser Part. Beams **18**(4), 661–695 (2000)
20. C. Phipps, C. Bonnal, F. Masson, M. Boustie, L. Berthe, M. Schneider, S. Baton, E. Brambrink, J.-M. Chevalier, L. Videau and S. A. E. Boyer, Transfers from Earth to LEO and LEO to interplanetary space using lasers, Acta Astronaut. **146**, 92–102 (2018)
21. J. Mason et al., Orbital debris-debris collision avoidance. Adv. Space Res. **48**, 1643–1655 (2011)
22. D. Overbye, *Reaching for the Stars, Across 4.37 Light-years*, New York Times 12 April 2016
23. C. Phipps, Comparing Laser and Electric Propulsion, in *Proceeding 4th International Workshop on Space Debris Modeling and Remediation*, Paris, 6–8 June 2016
24. C.R. Phipps Jr, T.P. Turner, R.F. Harrison, G.W. York, W.Z. Osborne, G.K. Anderson, X.F. Corlis, L.C. Haynes, H.S. Steele, K.C. Spicochi, T.R. King, Impulse Coupling to Targets in Vacuum by KrF, HF and CO2 Lasers. J. Appl. Phys. **64**, 1083 (1988)
25. C. Phipps et al., Removing orbital debris with lasers. Adv. Space Res. **49**, 1283–1300 (2012)
26. B. Poling et al., *The Properties of Gases and Liquids*, 5th edn. (McGraw-Hill, New York, 2001), pp. 7.9–7.11
27. The SESAME equation-of-state database is maintained by group T-1 at Los Alamos National Laboratory (sesame@lanl.gov); see S.P. Lyon and J.D. Johnson, SESAME: The Los Alamos National Laboratory Equation of State Database, LANL Report No. LA-UR-92-3407, 1992 for additional information
28. J. Sinko, C. Phipps, Modeling CO_2 laser ablation impulse of polymers in vapor and plasma regimes. Appl. Phys. Lett. **95**, 131105 (2009)
29. C. Phipps, An alternate treatment of the vapor-plasma transition. Int. J. Aero. Innovations **3**, 45–50 (2011)
30. C. Phipps, High power laser systems for space debris clearing, in *Fifth International School on Lasers in Material Science,* San Servolo, 10–17 July 2016
31. M. Saha, Ionization in the solar chromosphere. Phil. Mag. **40**, 472 (1920)
32. C.R. Phipps, C. Bonnal, A spaceborne, pulsed UV laser system for re-entering or nudging LEO debris, and re-orbiting GEO debris. Acta Astronaut. **118**, 224–236 (2016)
33. C. Phipps, High Power Laser Systems for Space Debris Clearing, in *Fifth International School on Lasers in Materials Science*, San Servolo, Italy, 10–17 July 2016
34. K. Fournier, LASNEX calculations of laser-coupling coefficients for Al targets, UCRL-Pres-226849, p. 29 (2006)
35. E. Loktionov et al., Thermophysical and gas-dynamic characteristics of laser-induced gas-plasma flows under femtosecond laser ablation. Q. Electron. **44**, 225–232 (2014)
36. X. Zhu, N. Zhang, Investigation of ultrashort pulse laser propulsion using time-resolved shadowgraphy and torsion pendulum, in *Proceeding of International Symposium on Photoelectric Detection and Imaging*, SPIE 7382, 73208 (2009)
37. S. Scharring et al., Numerical simulations on laser-ablative micropropulsion with short and ultrashort laser pulses. Trans. JSASS Aerospace Tech. **14**, 69–75 (2016)
38. C. Phipps, Comparative Performance of Laser and Electric Space Propulsion, Final report, CNES document AVP-NT-3250000-ZZ-1606-CNRS (2016), available from CNES
39. C. Phipps, J. Luke, Diode laser-driven microthrusters: a new departure for micropropulsion. J. AIAA **40**(20), 310–318 (2002)
40. C. Phipps, M. Boustie, J.-M. Chevalier, S. Baton, E. Brambrink, L. Berthe, M. Schneider, L. Videau, S.A.E. Boyer and S. Scharring, Laser impulse coupling measurements at 400 fs and 80 ps using the LULI facility at 1057 nm wavelength. J. Appl. Phys. **122**, 193103. (2017) https://doi.org/10.1063/1.4997196
41. R. Weber et al., Heat accumulation during pulsed laser materials processing. Opt. Express **22**, 11312–11324 (2014)

42. C. Phipps, L'ADROIT—a spaceborne ultraviolet laser system for space debris clearing. Acta Astronaut. **104**, 243–255 (2014)
43. Bosch working on 50 kWh battery pack weighting 190 kg, http://www.electric-vehiclenews.com/2015/10/bosch-working-on-50-kwh-battery-packs.html
44. C. Phipps, Pulsed Laser ADR Strategy, in talk #5.2, *3rd European Workshop on Space Debris Modeling and Remediation*, CNES-HQ, Paris, 16–18 June (2014)
45. C. Phipps et al., Small Payload Transfers from Earth to LEO and LEO to Interplanetary Space using Lasers, in *Proceeding of 7th European Conference for Aeronautics and Space Sciences*, Politecnico di Milano, Milan, 3–6 July 2017
46. R. Soulard et al., ICAN: a novel laser architecture for space debris removal. Acta Astronaut. **105**, 192–200 (2014)
47. C. Phipps, Concerns for Phased Fiber laser arrays in space, in *4th European Workshop on Space Dberis modeling and Remediation, CNES-HQ,* Paris, 6–8 June 2016
48. T. Ebisuzaki et al., Remediation of cm-size space debris from the International Space Station, in *Proceeding Workshop on Laser Solutions for Orbitral Debrs*, Université Paris Diderot, 27–28 April 2015
49. http://www.hilase.cz/en/advanced-dpssl-laser-dipole-100-delivers-1kw-performance/
50. C. Phipps, C. Bonnal, F. Masson and P. Musumeci, Launching swarms of microsatellites using a 100 kW average power pulsed laser, JOSA B **35**(10), B20–B26 (2018) https://doi.org/10.1364/JOSAB.35.000B20